Author(s): Lahtinen, Elmeri; Kukkonen, Esa Petteri; Jokivartio, Joonas; Parkkonen, Joni; Virkajärvi, Jussi; Kivijärvi, Lauri; Ahlskog, Markus; Haukka, Matti

Title: Preparation of Highly Porous Carbonous Electrodes by Selective Laser Sintering

Year: 2019

Version: Published version

Please cite the original version:

Lahtinen, E., Kukkonen, E. P., Jokivartio, J., Parkkonen, J., Virkajärvi, J., Kivijärvi, L., Ahlskog, M., & Haukka, M. (2019). Preparation of Highly Porous Carbonous Electrodes by Selective Laser Sintering. ACS Applied Energy Materials, 2(2), 1314-1318. https://doi.org/10.1021/acsaem.8b01881

ACS APPLIED ENERGY MATERIALS

Article

Cite This: ACS Appl. Energy Mater. 2019, 2, 1314−1318

www.acsaem.org

Preparation of Highly Porous Carbonous Electrodes by Selective Laser Sintering

Elmeri Lahtinen,[†] Esa Kukkonen,[†] Joonas Jokivartio,[‡] Joni Parkkonen,[§] Jussi Virkajärvi,[§] Lauri Kivijärvi,[†] Markus Ahlskog,[‡] and Matti Haukka*[,†]

[†]Department of Chemistry, University of Jyväskylä, P.O. Box 35, FI-40014 Jyväskylä, Finland

[‡]Department of Physics, Nanoscience Center, University of Jyväskylä, P.O. Box 35, FI-40014 Jyväskylä, Finland

[§]Department of Physics, University of Jyväskylä, P.O. Box 35, FI-40014 Jyväskylä, Finland

Supporting Information

ABSTRACT: Selective laser sintering (SLS) 3D printing was utilized to fabricate highly porous carbonous electrodes. The electrodes were prepared by using a mixture of fine graphite powder and either polyamide-12, polystyrene, or polyurethane polymer powder as SLS printing material. During the printing process the graphite powder was dispersed uniformly on the supporting polymer matrix. Graphite's concentration in the mixture was varied between 5 and 40 wt % to find the correlation between the carbon content and conductivity. The graphite concentration, polymer matrix, and printing conditions all had an impact on the final conductivity. Due to the SLS printing technique, all the 3D printed electrodes were highly porous. By using polyurethane as the supporting matrix it was possible to produce flexible electrodes in which the conductivity is sensitive to pressure and mechanical stress. Physical properties such as graphite distribution, attachment, and the overall porosity of the printed electrodes were studied using scanning electron microscopy (SEM), helium ion microscopy (HIM), and X-ray tomography. The results show that the combination of chemical design of the printing material and the utilization of SLS 3D printing enables fabrication of highly customizable electrodes with desired chemical, physical, mechanical, and flow-through properties.

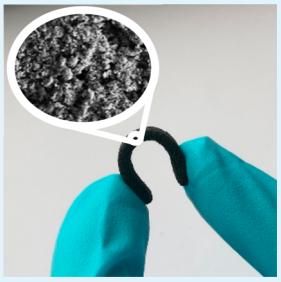

KEYWORDS: *porous electrodes, 3D printing, selective laser sintering, conductivity, graphite*

INTRODUCTION

Increasing demand for high performance batteries in a wide variety of electronic applications from portable electronic devices to electric cars has generated a need for new approaches in battery design.[1,2] Especially, the development of novel electrodes has gained a lot of interest.[3−5] Obviously, the most important property of an electrode is its conductivity, but other features such as surface area and porosity can also have a significant impact on the electrodes' electrochemical properties and their applicability from more conventional systems to redox flow batteries.[6] When considering a typical graphite electrode, the achievable surface area consists only of the outer layer of the electrode; the inner parts of the electrode are not accessible. Several methods to increase the surface area have been proposed, including the addition of nanomaterials into the graphite, the usage of different templating methods, and the use of organic monolayered additives.[7−12]

During the past decade, three-dimensional printing has also been exploited in fabrication of highly customizable electrochemical devices.[13,14] Several papers have been published for examples of 3D printed graphene-based electrodes and microbatteries.[15−20] In these studies, three-dimensional printing has enabled a rapid production of components and devices for electrochemical applications. However, in most cases the 3D printing technique used has been either the fused deposition modeling (FDM) or direct ink writing (DIW), while other 3D printing techniques have received little to no interest. Both FDM and DIW produce surfaces that are not inherently porous, and the methods often require specifically customized printing materials. In principle, a wide range of commercial materials are available, but fine-tuning these printing materials for specific applications while simultaneously trying to match the requirements of a specific printing method can be laborious and demanding. From this point of view, powder-based methods, such as selective laser sintering (SLS), can provide a way to avoid some of these pitfalls. For example, with the SLS 3D printing technique, it is possible to produce objects that are inherently porous. In SLS printing, small particles with a typical diameter of 50−100 μm are fused together by a laser which gives, at least up to a point, control over the physical characteristics such as the porosity and mechanical strength of the material by fine-tuning the printing parameters such as laser power, exposure time, and printing temperature.[21−24] When the particles are sintered in such a way that only their surfaces are partially melted, a solid structure containing accessible voids between the sintered grains is obtained. With powder-based methods, it is also relatively easy to add functional additives into the printed

Received: November 1, 2018
Accepted: January 10, 2019
Published: January 10, 2019

DOI: 10.1021/acsaem.8b01881
ACS Appl. Energy Mater. 2019, 2, 1314−1318

object by simply mixing the additive with the printable matrix. If the matrix particles are only partially sintered, the additive is dispersed on the surface of these particles and therefore accessible by fluids flowing through the printed object enabling applications such as porous flow-through columns for scavenging metal ions from aqueous solutions.[25] The SLS technique also allows the alteration of physical properties such as the density of the printed objects within the object itself. This means that different areas of the 3D printed object can be tuned to have different porosities and objects with well-defined permeable and impermeable areas can be made.[25] This in turn broadens the range of plausible applications for the printed objects.

In SLS 3D printing, the most commonly used printing materials are simple polymers such as polyamides, polypropylene, or polystyrene. These polymers are nonconductive by nature and therefore not suitable as electrode materials. Obviously, conducting polymers could be used to obtain electrodes. However, the chemical nature of the electrode is also dependent on the material. Furthermore, the conductive polymers are often relatively expensive.[26] Therefore, use of a conductive component only as an additive seems like an appealing option. The SLS technique sets only minimal requirements for the choice of the functional additives as nearly any components can be mixed within the matrix powder. There is a wide range of different conductive components available, from conductive polymers to carbon nanotubes and metals, which could potentially be used as conductive additives. Simple graphite, however, is a good example of an additive that possesses conductivity and is still rather cost-efficient. In this work, graphite powder mixed into either polyamide-12, polystyrene, or polyurethane matrix was used for preparation of highly porous carbonous electrodes using SLS 3D printing. The graphite content plays a key role in the conductivity, and therefore, the impact of the graphite concentration was investigated to find the optimum graphite/matrix ratio.

RESULTS AND DISCUSSION

The printing material for the fabrication of the electrodes was prepared by mixing either commercial polystyrene, polyamide-12, or polyurethane powder with synthetic bulk graphite powder. The graphite content was varied between 5 and 40 wt % to find the optimum additive/matrix ratio. Electrodes with different shapes and sizes were designed for different analytical experiments. Square- and rectangle-shaped electrodes (Figure 1a) were used for the resistance measurements and for performing the helium ion microscopy (HIM)[27] and the scanning electron microscopy (SEM) imaging, whereas cylinder-shaped electrodes (Figure 1a) were prepared for the X-ray tomography analysis. Physical properties of the electrodes were fine-tuned by optimizing printing parameters such as layer thickness, laser power, and printing speed.

The amount of graphite in the powder mixture affects the required printing parameters. To obtain electrodes with sufficient mechanical strength and durability while retaining the porous structure requires adjusting the printing conditions for each graphite/matrix system. The structure of the printed electrodes and the distribution of graphite were studied using SEM, HIM, and X-ray tomography. The SEM images of the break surfaces of the 3D printed graphite/polystyrene electrodes are shown in Figure 1b–d. The set of SEM images of the graphite/polyamide-12 electrodes also display similar

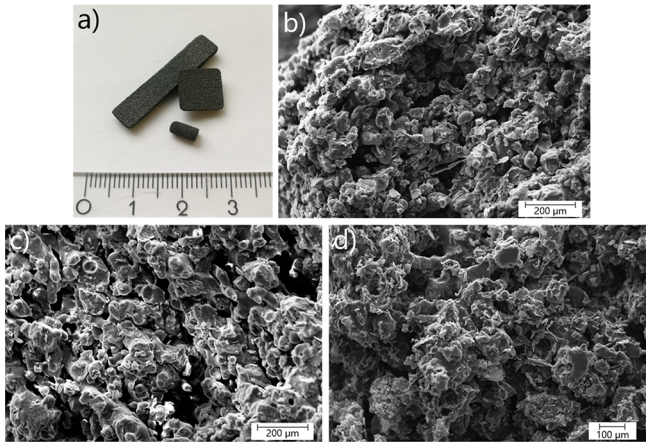

Figure 1. Rectangle-, square-, and cylinder-shaped, polystyrene-based SLS 3D printed electrodes with 30 wt % of graphite (a). SEM image of the break surface of 3D printed polystyrene electrode with 20 wt % (b), 30 wt % (c), and 40 wt % (d) of graphite.

structural characteristics (Figures S1–S4). The images reveal the highly macroporous structure of the material, in which the graphite powder is distributed evenly throughout the objects. As can be seen, the polymer particles have been only partially fused together by the sintering process, thus forming the porous structure with accessible voids between the particles.

To avoid any problems caused by possible charging of the material during the SEM imaging, the 3D printed electrodes were also analyzed by helium ion microscopy (Figure 2). The HIM images confirmed the highly macroporous structure of the electrodes, but they also clearly show graphite's attachment on the surface of the polymeric three-dimensional network (Figure 2a). In the SLS 3D printing process, it is possible to

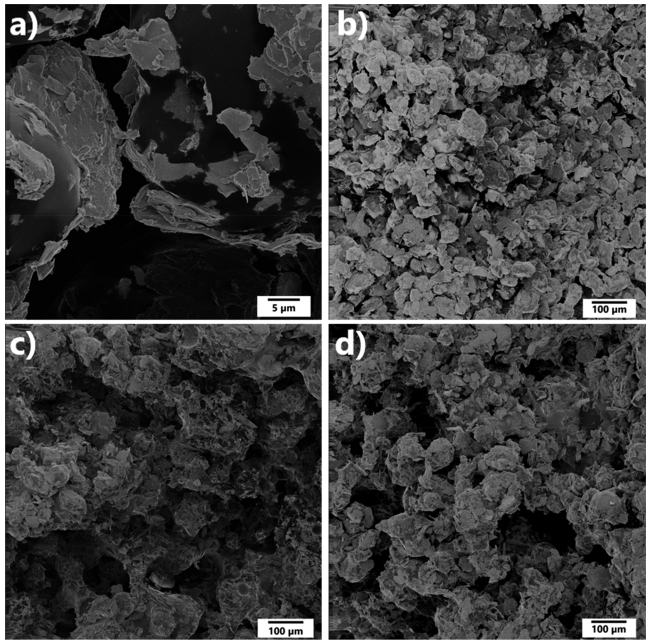

Figure 2. Helium ion microscope (HIM) image of the break surface of the 3D printed polystyrene electrode having 20 wt % of graphite, showing that the graphite flakes are covering the surface of the partially melted polystyrene matrix (a). HIM image of the break surface of the 3D printed polystyrene electrode with 20 wt % (b), 30 wt % (c), and 40 wt % (d) of graphite.

DOI: 10.1021/acsaem.8b01881
ACS Appl. Energy Mater. 2019, 2, 1314–1318

obtain objects where the additive is not entirely capsulated by the matrix, but it is firmly attached only on the matrix's partially melted surface of the polymer matrix. This means that the additive is not just loosely trapped within the three-dimensional structure; it is strongly anchored onto the polymeric matrix. On the other hand, the additive is achievable by fluids, gases, or liquids, passing through the porous material.

To confirm that the images of the outer layer and the break surfaces obtained via HIM and SEM imaging represent the overall internal structure of the electrodes, X-ray tomography of the electrodes was carried out. For these analyses, electrodes with 30 wt % of graphite were used. The tomography images (Figure 3) show that the whole electrode is porous and that

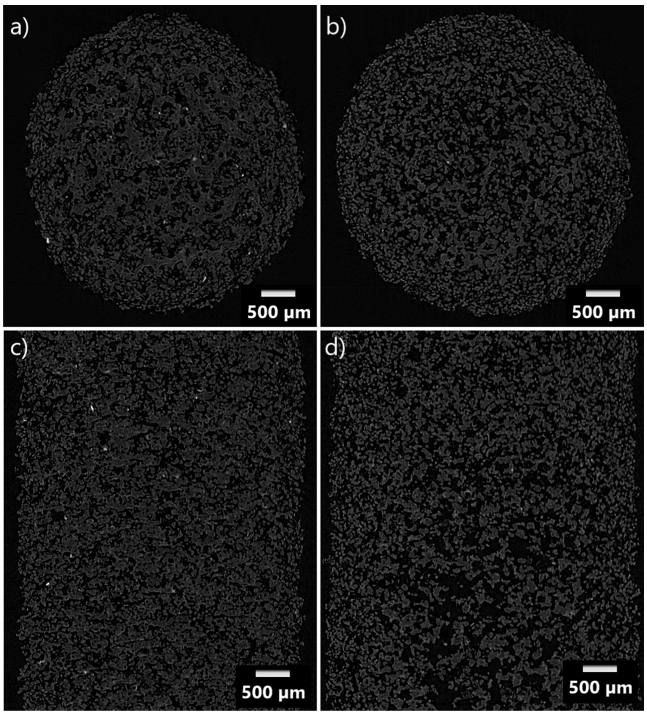

Figure 3. Horizontal slice of the structure of the cylinder-shaped SLS printed electrode from X-ray tomography analysis of polystyrene-based (a) and polyamide-12-based (b) electrodes having 30 wt % of graphite. Vertical slices of the X-ray tomography images of the polystyrene-based (c) and polyamide-12-based (d) electrodes having 30 wt % of graphite.

the structure observed from the HIM and the SEM images describes the structure well. The structural analyses confirmed that porous electrodes can be obtained with both polystyrene and polyamide-12. The detailed analysis of the X-ray tomography results showed that the macroporous structure of the polystyrene electrode has 41% empty space inside the electrode whereas the polyamide-12-based electrode has 49% empty space. Analysis of the average pore diameter indicated that the polystyrene and polyamide-12 electrodes have average pore diameters between 10−55 and 10−75 μm, respectively (Figures S5 and S6).

The printed electrodes can be used as electrodes for example for conventional electrolysis. However, in such a case the electrochemical processes take place on the outermost surface of the electrode (Figures S7 and S8). The full advantage of the printed electrodes can be obtained when they are used as flow-through electrodes for example in flow batteries (Figure S9). By printing, it is possible to fine-tune the flow properties by adjusting the printing conditions or by printing optimized flow channels with desired diameter and shape throughout the electrodes.

In addition to more rigid polystyrene and polyamide electrodes, polyurethane-based graphite electrodes were 3D printed to obtain flexible and fully bendable, but still porous and conductive, objects (Figure S10). The flexible electrodes were printed using 30 wt % of graphite mixed with polyurethane powder. The inherent porosity of the SLS printed material and the elastic nature of the polymer led to an object whose conductivity could be reversibly changed by applying pressure to it (Figure S11). When the flexible material is compressed, the graphite particles, scattered on the surfaces of the polymer beads, are pressed together, which lowers the resistance and increases the conductivity. The change is considerable and can be easily measured. Such behavior opens up the possibility of using the material as a simple pressure sensor or a sensor for mechanical stress. Even though closely related piezoresistive materials are known and widely reported,[28−31] SLS 3D printing could provide an alternative method to prepare objects with pressure/conductivity correlation.

Conductivities of the rigid electrodes were studied in detail by using a high resistance meter. From the conductivities of the graphite/polystyrene electrodes (Figure 4), it can be seen that

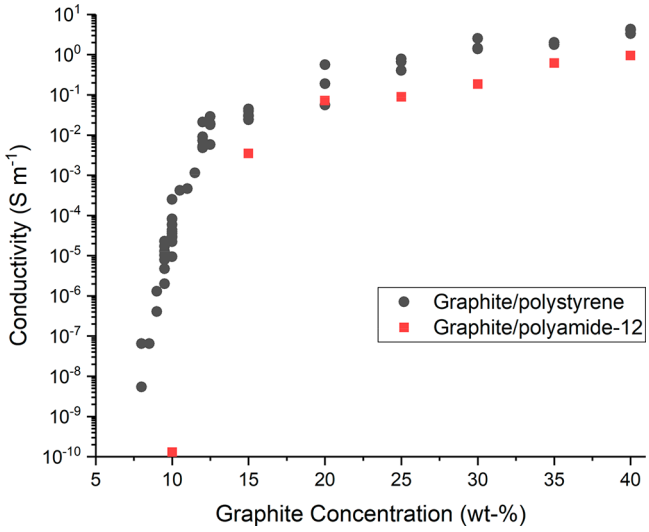

Figure 4. Conductivities of the 3D printed PS and PA12 electrodes as a function of the graphite concentration measured at 300 K.

the conductivity increases rapidly when the graphite concentration is raised from 7.5 to 15 wt %, indicating that in these samples the conductivity jumps after the graphite concentration is high enough to produce firm graphite−graphite contacts in the material. It is likely that only certain chains of graphite−graphite contacts participate in the actual conduction paths, as stated in the percolation theory.[32] However, the printed electrodes contain enough of these chains to generate uniform behavior throughout the object. The increasing trend in conductivity then continues as the graphite concentration is increased further beyond 15 wt %. Naturally, the highest conductivity of 4.3 S m^{-1} is observed with the highest concentration of graphite. A similar trend can be seen in the conductivities of the graphite/PA12 electrodes

DOI: 10.1021/acsaem.8b01881
ACS Appl. Energy Mater. 2019, 2, 1314−1318

as they also seem to possess a rather sharp threshold for the conductivity between 10 and 15 wt %. The highest observed conductivity was 0.9 S m^{-1}, which is considerably less than that observed for the PS-based electrodes.

To obtain a reference point and a limiting maximum conductivity for the results, tightly packed compressed pellets were made of the graphite powder using a hydraulic press. The conductivities of the pure graphite pellets ranged between 55.1 and 70.8 S m^{-1}. The conductivities observed for the 3D printed electrodes are an order of magnitude lower than those observed for the pure graphite pellets, but obviously, the controllable porosity, shape, sizes, and flow properties are not achievable by the compressed pellets.

The results highlight the usability of the SLS 3D printing technique in the preparation of highly customizable porous carbonous electrodes. It should be noted that the electrodes fabricated here are not optimized to obtain the maximum conductivity. A low cost carbon additive with a rather small inherent conductivity was utilized for the study, meaning that the electric properties of the electrodes could be significantly increased by customization of the material itself. However, even these simple electrodes are already fully functional and can be used in electrochemical processes. It is more than likely that the full advantage could be achieved in processes where the porosity and flow-through properties can be utilized. One such potential application could be flow batteries.

DISCUSSION

The SLS 3D printing provides a way to easily fabricate highly customizable electrodes even by using low cost materials. The 3D printing technique gives the possibility to fine-tune the mechanical parameters such as the porosity and the flexibility of the electrodes by altering the supporting matrix material and the printing conditions. The technique is able to produce durable electrodes with high porosity and sufficient conductivity compared to the bulk graphite. Even though the study focused on graphite as the additive and common polymers as matrices, the method is not limited to these to materials and could be expanded to use different additives and polymers.

By using other additives such as conductive polymers or other carbon sources, or maybe even metals as well as choosing other types of supporting matrices, including conductive materials, the properties of the printed electrodes could be tuned and enhanced further. The possibility to tailor and design highly porous electrodes with well-defined conductivity and flow properties could open up a whole new way to fabricate highly efficient electrodes.

EXPERIMENTAL SECTION

Materials. The graphite used for preparation of the starting material was synthetic graphite powder (<20 μm) purchased from Sigma-Aldrich. The polymer powders with average particle diameters of 50 μm were purchased from ADVANC3D Materials. All chemicals were used as received.

Three-Dimensional Printing. The 3D models of electrodes were designed using FreeCAD v.0.16 software after which they were sliced into two-dimensional, 0.1 mm thick, slices using Slic3r v. 1.2.9. Electrodes were printed with a Sharebot SnowWhite SLS 3D printer. For preparation of the polystyrene-based electrodes, the laser speed was varied between 200 and 1200 mm s^{-1}, depending on the amount of graphite in the mixture, with powder temperatures between 106 and 108 °C and CO_2 laser power of 14 W. For polyurethane, similar settings were used, but the temperature was set to 121 °C. Polyamide-12-based electrodes were fabricated using laser speeds varying between 360 and 2560 mm s^{-1} and temperatures between 160 and 167 °C with laser power varying between 4 and 14 W. The 3D printing settings were adjusted for different graphite contents to obtain sufficient mechanical properties. The printed objects were carefully cleaned of all unsintered powder before using them in experiments.

Helium Ion Microscopy and Scanning Electron Microscopy. Helium ion microscopy was performed using a Carl Zeiss ORION NanoFab instrument. The beam energy used was around 30 kV with beam current ranging from 0.242 to 0.303 pA. A scan dwell time of 0.2 μs was used. A flood gun was used to counteract the charging effect. For HIM imaging, samples did not receive any additional pretreatment after the 3D printing process. Scanning electron microscopy was performed using a Zeiss EVO-50XVP instrument with accelerating voltage of 25 kV. Prior to SEM imaging, the 3D printed electrodes were coated with gold for optimal picture quality.

X-ray Tomography. X-ray tomographic imaging of the electrodes was carried out using a SkyScan 1172 microtomograph. Two cylinder-shaped samples of 4−5 mm in diameter were imaged with a 3.0 μm pixel size. The scanning parameters for both samples were identical. The X-ray source parameters were 29 kV and 100 μA, and no filter was used. A total of 1200 projection images were taken using a 0.3° step size over 360° of rotation. Projection images were averaged over 4 exposures of 4712 ms resulting in a total exposure time of 18.85 s for each of them. A total scan duration was 8 h. Tomographic images were reconstructed using NRecon software, which is based on the Feldkamp algorithm.[33] One pixel postalignment was needed for ideal reconstruction. No ring artifact correction or beam hardening correction was used. A total sample height that was reconstructed was 5.6 mm for both samples. To measure the relative porosity of the samples, the volumes of the pore structures and the total volumes of the samples were analyzed from the X-ray tomography images similarly, using ImageJ software. Additional information about the analysis is presented in Supporting Information.

Conductivity Measurements. A Keithley 6517A electrometer/high resistance meter was used to measure the resistance at room temperature. An attempt to minimize contact resistance was made by connecting copper plates to the sample with carbon black paste. Xylene was used as a solvent in carbon black paste. Copper wires were soldered to the plates, and the wires were ran into the measuring apparatus. Copper plates were scratched with sand paper to get rid of the oxide layer and to increase the contact area. High resistance samples were also soldered inside a shielded box so that coaxial wires came out of the box and were connected to the apparatus. Carbon black paste was applied as viscous as possible to prevent the paste from entering the pores of the material.

ASSOCIATED CONTENT

Supporting Information

The Supporting Information is available free of charge on the ACS Publications website at DOI: 10.1021/acsaem.8b01881.

Detailed description of X-ray tomography analysis as well as pore structure distribution graphs, additional SEM images, images of 3D printed electrodes being used for electrolysis and in a flow cell, and images of flexible 3D printed electrodes (PDF)

AUTHOR INFORMATION

Corresponding Author

*E-mail: matti.o.haukka@jyu.fi.

ORCID

Markus Ahlskog: 0000-0003-3479-2619

Matti Haukka: 0000-0002-6744-7208

DOI: 10.1021/acsaem.8b01881
ACS Appl. Energy Mater. 2019, 2, 1314−1318

Author Contributions

M.H. conceptualized the idea of the SLS 3D printed electrodes. E.L. and E.K. did the designing and the 3D printing of the electrodes. J.J. performed the conductivity experiments for the electrodes. M.A. supervised the conductivity measurements. J.P. and J.V. performed the X-ray tomography and the analysis of the results. L.K. assisted in the design and fabrication of the flexible electrodes. E.L. wrote the initial manuscript which was jointly revised.

Notes

The authors declare no competing financial interest.
The data supporting the findings of this study is available from the corresponding author upon reasonable request.

■ ACKNOWLEDGMENTS

Financial support from the Centennial Foundation of Technology industries of Finland and Jane and Aatos Erkko foundation is greatly appreciated. The research was also supported by the Academy of Finland (grant number: 295581 (M.H.)) and University of Jyväskylä.

■ REFERENCES

(1) Armand, M.; Tarascon, J.-M. Building Better Batteries. *Nature* **2008**, *451*, 652−657.
(2) Larcher, D.; Tarascon, J.-M. Towards Greener and More Sustainable Batteries for Electrical Energy Storage. *Nat. Chem.* **2015**, *7*, 19−29.
(3) Aricò, A. S.; Bruce, P.; Scrosati, B.; Tarascon, J.-M.; van Schalkwijk, W. Nanostructured Materials for Advanced Energy Conversion and Storage Devices. *Materials for Sustainable Energy* **2010**, 148−159.
(4) Kim, K. S.; Zhao, Y.; Jang, H.; Lee, S. Y.; Kim, J. M.; Kim, K. S.; Ahn, J.-H.; Kim, P.; Choi, J.-Y.; Hong, B. H. Large-Scale Pattern Growth of Graphene Films for Stretchable Transparent Electrodes. *Nature* **2009**, *457*, 706−710.
(5) Wang, F.; Wu, X.; Yuan, X.; Liu, Z.; Zhang, Y.; Fu, L.; Zhu, Y.; Zhou, Q.; Wu, Y.; Huang, W. Latest Advances in Supercapacitors: From New Electrode Materials to Novel Device Designs. *Chem. Soc. Rev.* **2017**, *46*, 6816−6854.
(6) Li, B.; Nie, Z.; Vijayakumar, M.; Li, G.; Liu, J.; Sprenkle, V.; Wang, W. Ambipolar Zinc-Polyiodide Electrolyte for a High-Energy Density Aqueous Redox Flow Battery. *Nat. Commun.* **2015**, *6*, 6303.
(7) Bruce, P. G.; Scrosati, B.; Tarascon, J.-M. Nanomaterials for Rechargeable Lithium Batteries. *Angew. Chem., Int. Ed.* **2008**, *47*, 2930−2946.
(8) Cho, C.-Y.; Moon, J. H. Hierarchically Porous TiO2 Electrodes Fabricated by Dual Templating Methods for Dye-Sensitized Solar Cells. *Adv. Mater.* **2011**, *23*, 2971−2975.
(9) Yoon, S.; Oh, S. M.; Lee, C. W.; Ryu, J. H. Pore Structure Tuning of Mesoporous Carbon Prepared by Direct Templating Method for Application to High Rate Supercapacitor Electrodes. *J. Electroanal. Chem.* **2011**, *650*, 187−195.
(10) Doherty, C. M.; Caruso, R. A.; Smarsly, B. M.; Drummond, C. J. Colloidal Crystal Templating to Produce Hierarchically Porous LiFePO4 Electrode Materials for High Power Lithium Ion Batteries. *Chem. Mater.* **2009**, *21*, 2895−2903.
(11) Park, J.; Lee, W. H.; Huh, S.; Sim, S. H.; Kim, S.; Cho, K.; Hong, B. H.; Kim, K. S. Work-Function Engineering of Graphene Electrodes by Self-Assembled Monolayers for High-Performance Organic Field-Effect Transistors. *J. Phys. Chem. Lett.* **2011**, *2*, 841−845.
(12) Yip, H.-L.; Hau, S. K.; Baek, N. S.; Ma, H.; Jen, A. K.-Y. Polymer Solar Cells That Use Self-Assembled-Monolayer- Modified ZnO/Metals as Cathodes. *Adv. Mater.* **2008**, *20*, 2376−2382.
(13) Ambrosi, A.; Pumera, M. 3D-Printing Technologies for Electrochemical Applications. *Chem. Soc. Rev.* **2016**, *45*, 2740−2755.
(14) Fu, K.; Yao, Y.; Dai, J.; Hu, L. Progress in 3D Printing of Carbon Materials for Energy-Related Applications. *Adv. Mater.* **2017**, *29*, 1603486.
(15) Sun, K.; Wei, T.-S.; Ahn, B. Y.; Seo, J. Y.; Dillon, S. J.; Lewis, J. A. 3D Printing of Interdigitated Li-Ion Microbattery Architectures. *Adv. Mater.* **2013**, *25*, 4539−4543.
(16) Fu, K.; Wang, Y.; Yan, C.; Yao, Y.; Chen, Y.; Dai, J.; Lacey, S.; Wang, Y.; Wan, J.; Li, T.; et al. Graphene Oxide-Based Electrode Inks for 3D-Printed Lithium-Ion Batteries. *Adv. Mater.* **2016**, *28*, 2587−2594.
(17) García-Tuñon, E.; Barg, S.; Franco, J.; Bell, R.; Eslava, S.; D'Elia, E.; Maher, R. C.; Guitian, F.; Saiz, E. Printing in Three Dimensions with Graphene. *Adv. Mater.* **2015**, *27*, 1688−1693.
(18) Reyes, C.; Somogyi, R.; Niu, S.; Cruz, M. A.; Yang, F.; Catenacci, M. J.; Rhodes, C. P.; Wiley, B. J. Three-Dimensional Printing of a Complete Lithium Ion Battery with Fused Filament Fabrication. *ACS Appl. Energy Mater.* **2018**, *1*, 5268−5279.
(19) Maurel, A.; Courty, M.; Fleutot, B.; Tortajada, H.; Prashantha, K.; Armand, M.; Grugeon, S.; Panier, S.; Dupont, L. Highly Loaded Graphite−Polylactic Acid Composite-Based Filaments for Lithium-Ion Battery Three-Dimensional Printing. *Chem. Mater.* **2018**, *30*, 7484−7493.
(20) Yao, B.; Chandrasekaran, S.; Zhang, J.; Xiao, W.; Qian, F.; Zhu, C.; Duoss, E. B.; Spadaccini, C. M.; Worsley, M. A.; Li, Y. Efficient 3D Printed Pseudocapacitive Electrodes with Ultrahigh MnO_2 Loading. *Joule* **2018**, DOI: 10.1016/j.joule.2018.09.020.
(21) Shi, D.; Gibson, I. Material Properties and Fabrication Parameters in Selective Laser Sintering Process. *Rapid Prototyp. J.* **1997**, *3*, 129−136.
(22) Shirazi, S. F. S.; Gharehkhani, S.; Mehrali, M.; Yarmand, H.; Metselaar, H. S. C.; Adib Kadri, N.; Osman, N. A. A. A Review on Powder-Based Additive Manufacturing for Tissue Engineering: Selective Laser Sintering and Inkjet 3D Printing. *Sci. Technol. Adv. Mater.* **2015**, *16*, 033502.
(23) Fina, F.; Goyanes, A.; Gaisford, S.; Basit, A. W. Selective Laser Sintering (SLS) 3D Printing of Medicines. *Int. J. Pharm.* **2017**, *529*, 285−293.
(24) Dizon, J. R. C.; Espera, A. H.; Chen, Q.; Advincula, R. C. Mechanical Characterization of 3D-Printed Polymers. *Addit. Manuf.* **2018**, *20*, 44−67.
(25) Lahtinen, E.; Hänninen, M. M.; Kinnunen, K.; Tuononen, H. M.; Väisänen, A.; Rissanen, K.; Haukka, M. Porous 3D Printed Scavenger Filters for Selective Recovery of Precious Metals from Electronic Waste. *Adv. Sustain. Syst.* **2018**, *2*, 1800048.
(26) Novák, P.; Müller, K.; Santhanam, K. S. V.; Haas, O. Electrochemically Active Polymers for Rechargeable Batteries. *Chem. Rev.* **1997**, *97*, 207−282.
(27) Joens, M. S.; Huynh, C.; Kasuboski, J. M.; Ferranti, D.; Sigal, Y. J.; Zeitvogel, F.; Obst, M.; Burkhardt, C. J.; Curran, K. P.; Chalasani, S. H.; et al. Helium Ion Microscopy (HIM) for the Imaging of Biological Samples at Sub-Nanometer Resolution. *Sci. Rep.* **2013**, *3*, 3514.
(28) Konarova, M.; Aslam, W.; Ge, L.; Ma, Q.; Tang, F.; Rudolph, V.; Beltramini, J. N. Enabling Process Intensification by 3 D Printing of Catalytic Structures. *ChemCatChem* **2017**, *9*, 4132−4138.
(29) Petchartee, S.; Monkman, G. Optimisation of Prehension Force through Tactile Sensing. *Ind. Rob.* **2008**, *35*, 361−368.
(30) Russel, A. R. *Robot Tactile Sensing*; Prentice-Hall: Brisbane, Australia, 1990.
(31) Yaniger, S. I. Force Sensing Resistors: A Review Of The Technology. *Electro International* **1991**, *1991*, 666−668.
(32) Kalaitzidou, K.; Fukushima, H.; Drzal, T. L. A Route for Polymer Nanocomposites with Engineered Electrical Conductivity and Percolation Threshold. *Materials* **2010**, *3*, 1089.
(33) Feldkamp, L. A.; Davis, L. C.; Kress, J. W. Practical Cone-Beam Algorithm. *J. Opt. Soc. Am. A* **1984**, *1*, 612−619.

DOI: 10.1021/acsaem.8b01881
ACS Appl. Energy Mater. 2019, 2, 1314−1318